AIAA-2003-4227

STAGE SEPARATION WIND TUNNEL TESTS OF A GENERIC TWO-STAGE-TO-ORBIT LAUNCH VEHICLE

Wayne J. Bordelon, Jr.*
Alonzo L. Frost*
Darren K. Reed‡
National Aeronautics and Space Administration
George C. Marshall Space Flight Center
Marshall Space Flight Center, AL 35812

Abstract

In support of NASA's Space Launch Initiative Program, stage separation wind tunnel tests of a generic two-stage-to-orbit (TSTO) launch vehicle were conducted to determine the interference aerodynamic forces and moments and to determine the proximity flow environment. The tests were conducted in the NASA Marshall Space Flight Center's Aerodynamic Research Facility using a manual separation fixture for a Mach number range of 2.74 to 4.96 and separation distances up to 80 percent and 35 percent of the body length in the vehicle X and Z coordinates, respectively. For the TSTO bimese, winged-body vehicle configuration, both wing-to-wing and wing-to-fuselage configurations were tested. Individual-body force and moment, schlieren, and surface pressure data were acquired. The results showed that the proximity aerodynamics were dominated by complex bow shock interactions, and that he booster was statically unstable at several separation positions. As compared to the isolated body, the proximity normal force change with pitch angle was found to be nearly the same, and the proximity axial force increased, in general, by 3% for both bodies.

Introduction

The Space Launch Initiative (SLI) Program was funded to develop the technologies and requirements needed for the design and development of a 2nd generation launch vehicle to improve the safety and reduce the cost of earth-to-orbit, manned space transportation. As part of that program, the Airframe Project was responsible for developing technologies related to launch vehicle airframes including aerodynamics and aerothermodynamics. One key technology required by TSTO launch vehicles is stage separation aerodynamics. A task entitled, "Stage Separation and Ascent Aerothermodynamics" was initiated to develop the tools and preliminary databases in this technology area. Understanding the two-body aerodynamic interference is key to being able to design a winged TSTO with acceptable nominal and abort separation capability. Marshall Space Flight Center (MSFC) supported the Stage Separation Task by conducting wind tunnel tests and computational fluid dynamic (CFD) analyses on a generic, bimese TSTO configuration. A series of four tests were conducted over a period from July through September of 2002.

The objectives of the LGBB stage separation testing were:

1) Develop and demonstrate stage separation test hardware and methods applicable to SLI TSTO configurations.
2) Develop a preliminary database for a generic TSTO configuration for supersonic staging.
3) Develop and apply miniature pressure transducer technology on small-scale models to obtain steady and unsteady surface pressures.

This paper contains a description of the experimental approach, results for Mach 2.99 for a limited set of the separation points, a discussion of the results, and observations made from this work. This paper is not intended to be a comprehensive report on the stage separation tests conducted at MSFC, and work is still in progress to fully analyze the results at additional Mach numbers and to compare them to CFD results.

---

* MSFC Space Transportation Dir. and AIAA member
‡ MSFC Space Transportation Directorate member

Experimental Approach

Aerodynamic Research Facility

The NASA Marshall Space Flight Center Aerodynamic Research Facility (ARF) is an intermittent blow-down tunnel that operates using high-pressure air flowing from storage tanks to atmospheric or vacuum conditions. A picture of the ARF is shown in figure 1. The ARF can be configured with three different test sections for aerodynamic research: 14 inch by 14 inch transonic and supersonic sections for external aerodynamic research and a specialized test section designed to perform internal flow research. The transonic test section provides a Mach number range from 0.2 to 2.0. Mach numbers between 0.2 and 1.3 are obtained by using a variable diffuser. The transonic range from 0.95 to 1.3 is achieved through the use of plenum suction and perforated walls. Each Mach number above 1.3 requires a specific set of contoured nozzle blocks. A solid wall supersonic test section provides the entire range from Mach 2.74 to 5.0 with one set of automatically actuated contour nozzle blocks. Finally, the ARF has a specialized test section designed to perform internal compressible flow research such as rocket engine nozzle testing.

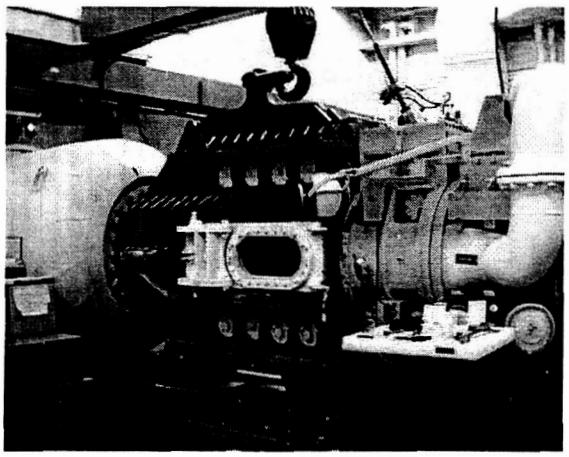

Figure 1. MSFC Aerodynamic Research Facility

A hydraulically controlled pitch sector located downstream of the test section provides the capability of testing model angles-of-attack from -10° to +10° during each run. Higher angles-of-attack are obtained with offset stings. On-line data is reduced to coefficient form by a solid-state data acquisition and computing system. More detailed information on the ARF may be obtained in reference 1.

Model Description

The models used for this investigation were approximately 1% scaled models of the Langley Glideback Booster (LGBB). This concept was developed by the NASA Langley Vehicle Analysis Branch to assess two-stage-to-orbit (TSTO) glideback booster aerodynamics. The LGBB was a conceptual winged-body configuration only, and it was not being considered as an SLI booster configuration. For the purpose of developing benchmark, generic TSTO stage separation data, two identical LGBB models were designed and fabricated to conduct bimese (aerodynamically identical) LGBB stage separation testing. A photograph of the models can be seen in figure 2. The models were modular with the canards (as shown), nose, wings, and tail being removable. The models were tested individually as "isolated" bodies as well as in "proximity" to each other to simulate TSTO separation. All the proximity cases were tested without canards. All major model components with the exception of filler blocks for the vertical tails are fabricated from stainless steel 17-4.

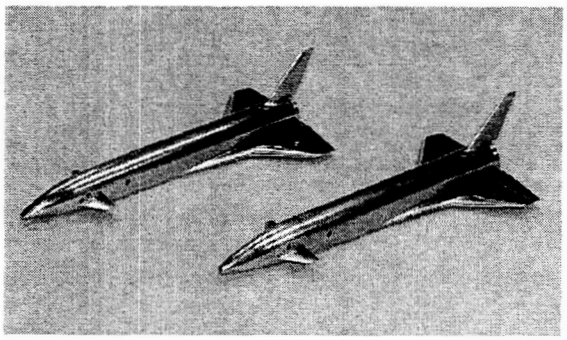

Figure 2. Models with Canards Installed

During the unsteady pressure measurement testing, the orbiter model was assembled with an instrumented wing-fuselage fitted with miniature pressure transducers (see the "Measurements, Instrumentation, and Data Acquisition Equipment" subsection below).

Model Mounting Hardware

The models were mounted inside the ARF on separate stings using a specially designed stage separation fixture installed in the tunnel pitch sector. Figure 3 shows a photograph of the models mounted in the tunnel. The stage separation fixture allowed for manual adjustment of the model's separation distance (del-X and del-Z) and relative pitch angle (del-alpha). The booster model (upper model) was,

in all tests, mounted on a sting with an internal force-moment balance. The orbiter model (lower model) was mounted on a sting with an active force-moment balance or with a hollow "dummy" balance designed to accommodate routing of the pressure transducer wire leads when the instrumented wing was installed. Isolated LGBB model (booster and orbiter) runs with an active balance were made with and without the stage separation fixture.

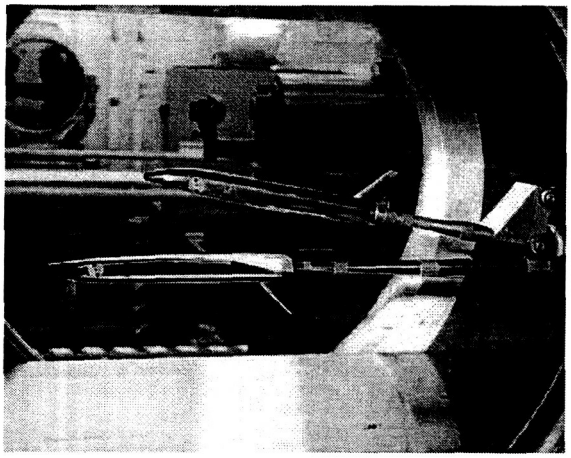

Figure 3. Models Mounted in ARF

Measurements, Instrumentation, and Data Acquisition Equipment

Two data acquisition systems were used for the tests: 1) the standard steady-state system for acquiring low frequency wind tunnel operating parameters, force-moment balance measurements, and model base pressures and 2) a high frequency Computer Aided Dynamic Data Measurement Acquisition System (CADDMAS) for acquiring unsteady pressures, tunnel reference conditions, and other unsteady parameters.

The CADDMAS is a 32 channel, 16 bit A/D system with a 5K samples per second frequency rate. The CADDMAS uses a parallel processor system with digital signal processors, analog-to-digital front-end processors, and standard personal computers. Using a parallel processing approach, the system achieves supercomputer performance in an interactive, high data bandwidth environment.

The LGBB orbiter model wing-fuselage component was instrumented with twenty (20) miniature pressure transducers. A photograph of the instrumented wing-fuselage is given in figure 4. Figure 4 shows the wing windward side only, but transducers were located on both the windward and leeward sides. The pressure transducers were mounted with epoxy into specially designed pockets machined into the part, and then the epoxy was machined with the transducers in place to restore the aerodynamic surface. In figure 4, the gray areas are where epoxy was used to fill the wire routing and restore the wing surface. The transducer number labels were in place for the photograph in figure 4, but removed prior to testing. The transducer leads were routed on the wing side opposite the side where the transducers were located to minimize flow disturbance on the transducer. The white areas are the location of the transducers.

Force-moment measurements were made using standard ½ inch strain gaged balances powered by a 4-volt power supply. Base pressure data was also measured using a pressure scanning system to allow the calculation of forebody coefficients. The base pressures were measured by locating external tubes along the sting in the base area of the model.

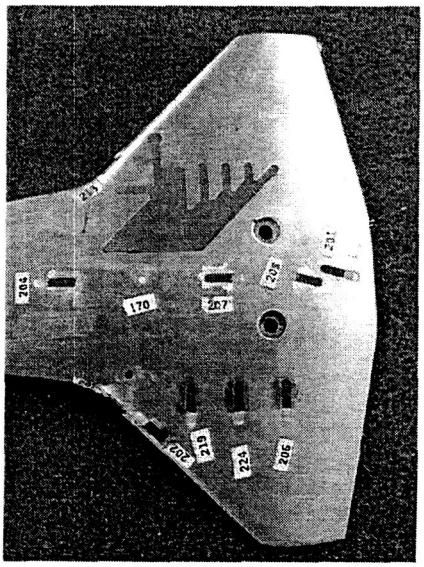

Figure 4. Instrumented Wing-Fuselage

Test Procedures and Data Reduction

At the ARF, a "run" consisted of a tunnel blowdown at one test condition. For separation testing, data was acquired at four sector angles: -4, -2, 0, +2, and +4 degrees during each run. The separation fixture, stings and both models moved with the sector with the orbiter pitch angle coinciding with the negative sector angle (since the orbiter was inverted) and the booster pitch angle determined by the configuration and the pre-run manual adjustment of the orbiter-booster relative pitch angle (del-alpha). The relative separation distance (del-X and del-Z) was also manually set prior to each run. The longitudinal coordinate system is depicted in figure 5. A standard body-fitted coordinate system was

used for each body. The orbiter coordinate system was adopted as the stack reference system.

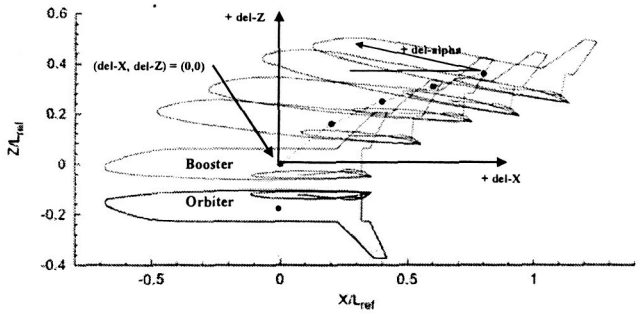

Figure 5. Pitch Plane Coordinate System

Data reduction consisted of the standard on-line calculation of the tunnel run conditions and reduction of the forces and moments to coefficient form. The on-line data reduction program also included sting-balance pitch angle deflection corrections to determine the wind-on angle-of-attack for each model. Off-line corrections were made to account for the change in the orbiter-booster relative position due to deflections of the balances, stings, and separation fixture with load. As with the pitch angle corrections, the relative position corrections were determined using pretest balance-sting-fixture deflection loadings for each configuration. These corrections were small, but significant in some cases. Finally, the on-line calculations are re-computed off-line using the raw tunnel measurements to verify their accuracy and make any run-time error corrections.

Test Conditions and Configurations

The LGBB models were tested in three basic configurations: 1) isolated orbiter or booster, 2) wing-to-wing proximity configuration, and 3) wing-to-fuselage proximity configuration. The isolated models were tested with and without canards over a range of Mach numbers from 0.3 to 4.96 and angles-of-attack (alpha) from –14 to +18 degrees. The isolated LGBB data without canards is included in this paper only as reference data for comparison to the proximity data.

The wing-to-wing configuration at a simulated separation point was shown in figure 3. This configuration was also referred to as the belly-to-belly configuration. Figure 6 is a photograph of the wing-to fuselage (or piggy-back) configuration in the "baseline" proximity or simulated TSTO stack position. In all cases, the top model simulated a booster separating from an inverted orbiter for the bimese LGBB TSTO vehicle. The models were tested without canards; and the booster model's vertical tail was removed for the wing-to-fuselage case. For the proximity configurations, data was acquired at the following test conditions:

Mach: 2.74, 2.99, 3.48, 4.45, and 4.96
Stack alpha: -4, -2, 0, +2, and +4 degrees
Del-alpha: 0, 5, and 10 degrees
Del-X/Lref: +0.0 to +0.8
Del-Z/Lref: -0.025 to +0.350

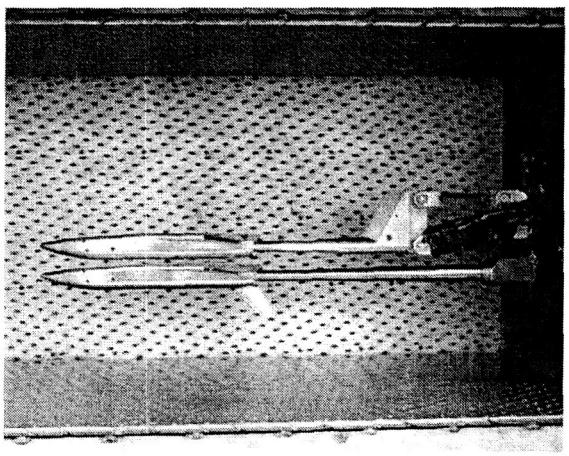

Figure 6. Wing-to-Fuselage Configuration

Results and Uncertainties

In this section, three types of data are presented: schlieren video still frame images, longitudinal force-moment coefficients, and unsteady surface pressures. As will be shown, the results are a function of: Mach number, orbiter (or stack) alpha, del-X, del-Z, and del-alpha. Only Mach 2.99 data for a subset of the separation points tested will be discussed in this paper. Since running the complete del-X, del-Z, and del-alpha matrix for each configuration was not required to meet the objectives of the task, trajectories or "slices" through the full separation matrix were tested and analyzed. For the wing-to-wing and wing-to-fuselage configurations, two of these so-called trajectories will be presented and discussed in this paper: 1) the Z trajectory and 2) the "sample" trajectory.

Schlieren Results

Figures 7 and 8 show the relative locations of the orbiter and booster for the Z and sample trajectories in the wing-to-wing configuration along with the schlieren images at each position. These trajectories are the same for the wing-to-fuselage configuration.

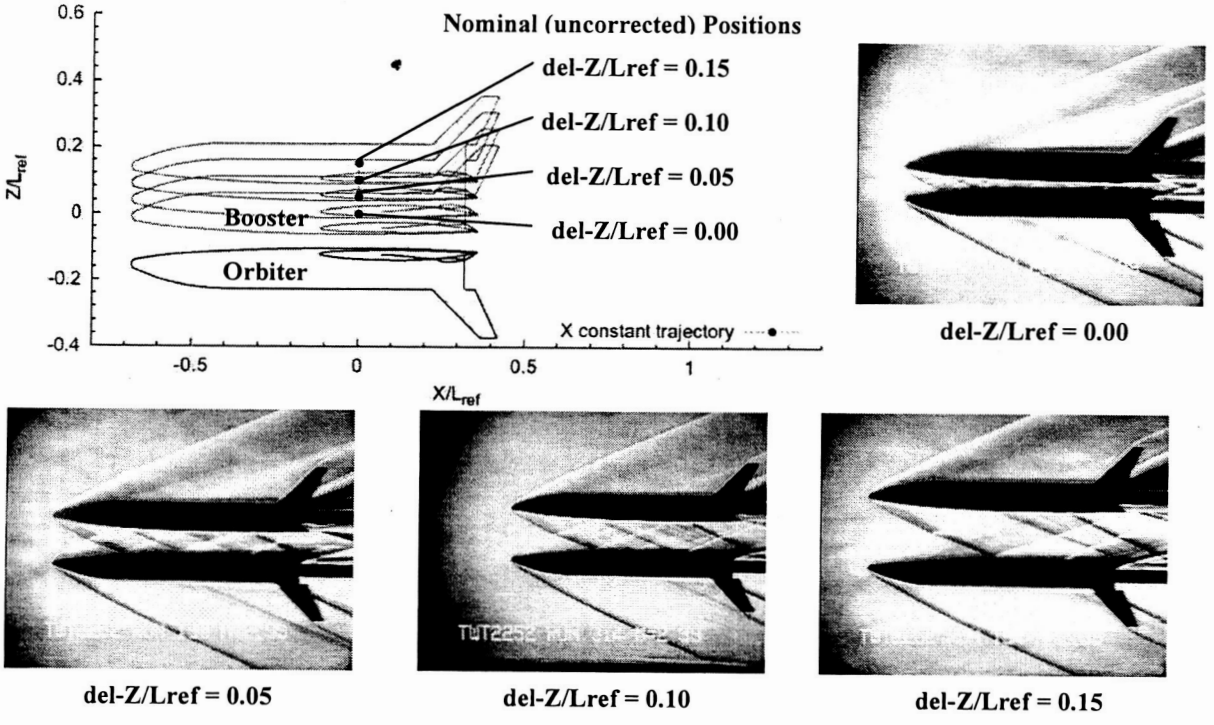

Figure 7. Wing-to-Wing, Z Trajectory Schlieren Video Still Frames

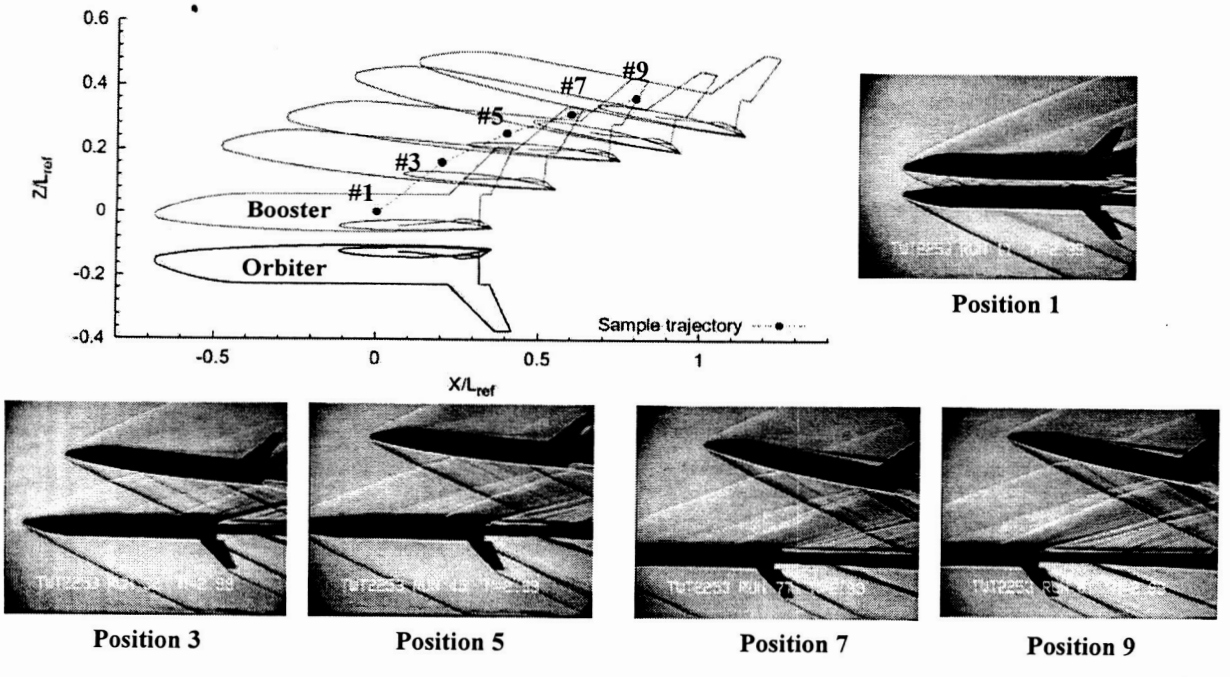

Figure 8. Wing-to-Wing, Sample Trajectory Schlieren Video Still Frames

The Z trajectory consisted of simply moving the booster to different del-Z positions with del-X and del-alpha remaining zero. On the other hand, the sample trajectory consisted of a simulated simultaneous change in del-X, del-Z, and del-alpha. For the sample trajectory, schlieren images are shown only for 5 of the 9 positions tested.

Force and Moment Results

For the force and moment results, the data is presented as a function of alpha and separation position. The uncertainties of the measured results were estimated, and the plot symbol sizes adjusted to represent the independent variable +/- uncertainty. The uncertainties were estimated by combining the balance calibration precision with the measurement repeatability determined from repeat runs to estimate a total measurement uncertainty. The estimated uncertainties were as follows:

Normal Force Coefficient = +/- 0.006
Pitching Moment Coefficient = +/- 0.0008
Axial Force Coefficient = +/- 0.003

The proximity force and moment increments were defined as follows:

$$\Delta C_{(\,)_{orbiter/booster}} = C_{(\,)_{orbiter/booster}} - C_{(\,)_{iso}}$$

where:

$C_{(\,)} = C_N, C_M, or\, C_A$

$\Delta C_{(\,)_{orbiter/booster}}$ = increment of $C_{(\,)}$ for orbiter in proximity to booster

$C_{(\,)_{orbiter/booster}}$ = $C_{(\,)}$ for orbiter in proximity to booster

$C_{(\,)_{iso}}$ = $C_{(\,)}$ for isolated LGBB

Similarly for the booster increment, we have:

$$\Delta C_{(\,)_{booster/orbiter}} = C_{(\,)_{booster/orbiter}} - C_{(\,)_{iso}}$$

Figures 9 and 10 are plots of the normal force coefficient and pitching moment coefficient as a function of alpha for the orbiter for the wing-to-wing configuration at the four Z trajectory positions. These plots represent the closest form of the data to the as acquired form, since alpha was varied during each run. The plots all include the isolated LGBB data and the measurement uncertainty estimate for reference. Since the wing-to-wing Z trajectory for all four positions is always a symmetrical proximity configuration, plots for the booster were very similar and not provided here.

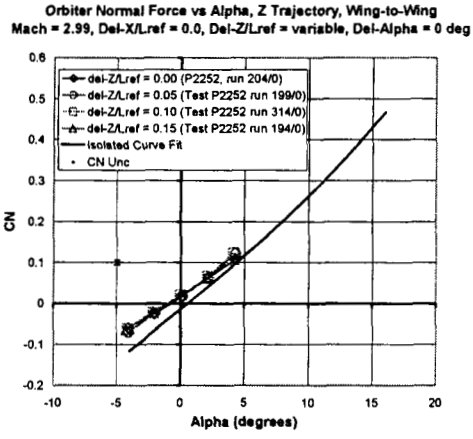

Figure 9. Orbiter Normal Force, Wing-to-Wing, Z Trajectory

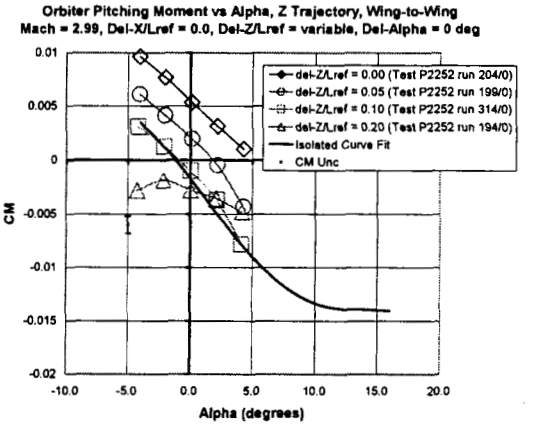

Figure 10. Orbiter Pitching Moment, Wing-to-Wing, Z Trajectory

Figures 11 and 12 are plots of the normal force and pitching moment increments, as defined above, for both the wing-to-wing and wing-to-fuselage configurations as a function of the non-dimensional Z position. These plots show results for the orbiter alpha = 0 degrees only, and they are cross plots of some of the data presented in figures 9 and 10. Additionally, figures 11 and 12 provide data for both the orbiter and booster confirming the symmetrical nature of this special separation case. The plots in figures 11 and 12 contain test-to-test repeat data, and the plot symbols are color-coded: blue for booster data and red for orbiter data.

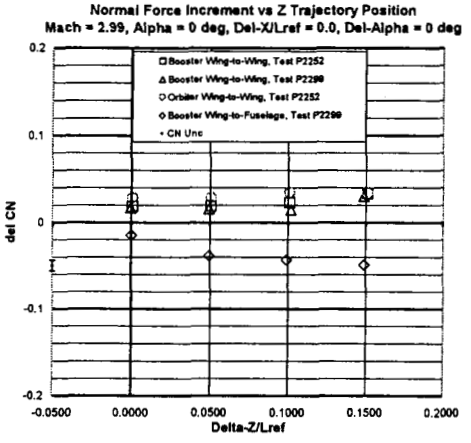

Figure 11. Normal Force Increment, Z Trajectory

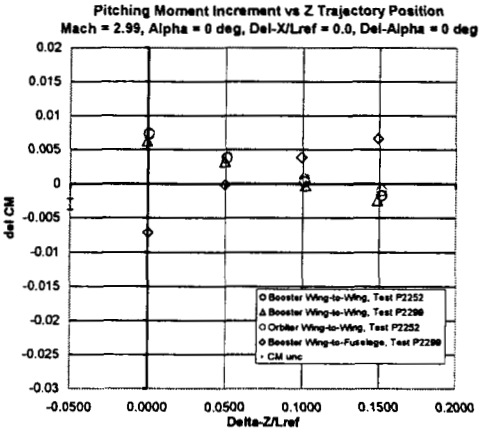

Figure 12. Pitching Moment Increment, Z Trajectory

Similar to figure 9, figures 13 and 14 are plots of the normal force coefficient as a function of alpha for the sample trajectory for the booster and orbiter, respectively. The sample trajectory is not a symmetrical separation case, so both the orbiter and booster data is provided. Here the data for the wing-to-wing and the wing-to-fuselage configurations are plotted on the same plot. The wing-to-wing data is plotted in blue and the wing-to-fuselage is plotted green. Also notice that the range of alpha varies for the different sample trajectory positions for the booster. Again, these plots depict more closely the as run variation in the independent parameters with alpha being varied during a run and del-X, del-Z, and del-alpha being changed manually between runs. For example, during run 61/0 of Test P2252 the orbiter was traversed through an alpha of –4 to +4 degrees while during the same run the booster's alpha traversed from +6 to +14 degrees for the wing-to-wing position 9 case.

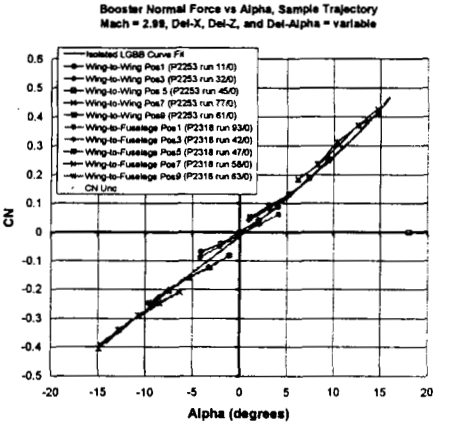

Figure 13. Booster Normal Force, Sample Trajectory

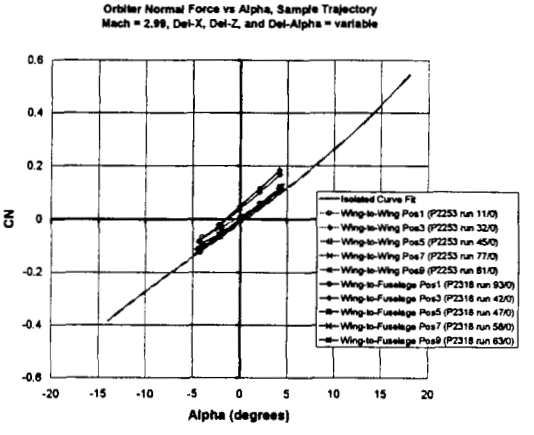

Figure 14. Orbiter Normal Force, Sample Trajectory

Similar to figure 10, figures 15 and 16 show the pitching moment versus alpha for the sample trajectory. It should be noted that the booster tail was removed for the wing-to-fuselage configuration. To quantify this effect, runs of the isolated LGBB were conducted without the vertical tail. As expected, the removal of the vertical tail had little effect of the normal force, but the pitching moment and axial force were significantly reduced. The booster proximity pitching moment and axial force could not be corrected to approximate the booster aerodynamics as if a tail were installed; however, the normal force and pitching moment increments were adjusted by using the isolated, no-tail results for the booster. This was accomplished by subtracting the no-tail isolated data from the no-tail booster proximity data.

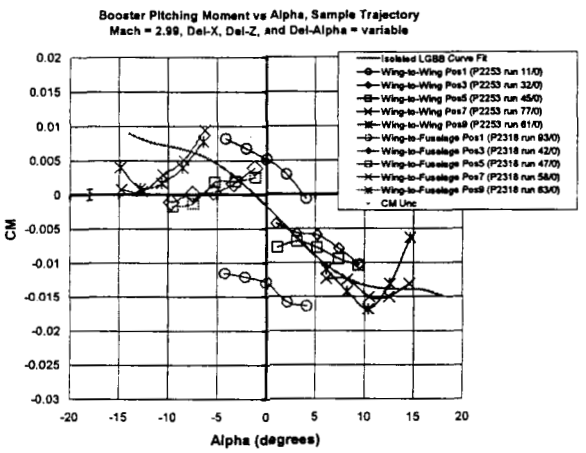

Figure 15. Booster Pitching Moment, Sample Trajectory

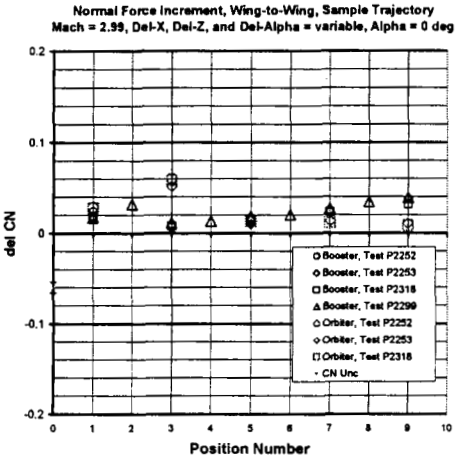

Figure 17. Normal Force Increment, Wing-to-Wing, Sample Trajectory

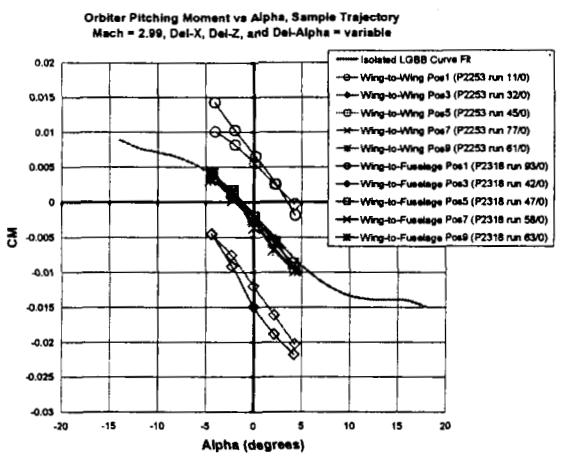

Figure 16. Orbiter Pitching Moment, Sample Trajectory

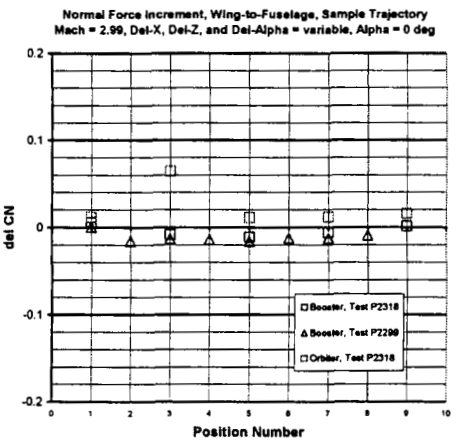

Figure 18. Normal Force Increment, Wing-to-Fuselage, Sample Trajectory

Similar to figures 11 and 12, figures 17, 18, 19, and 20 are plots of the normal force and pitching moment increments at alpha = 0 versus the sample trajectory position. The wing-to-wing and wing-to-fuselage configurations are shown on separate figures, but both the orbiter and booster increments are shown along with repeat test data where available. It should be noted that during test P2299, a higher resolution sample trajectory was run with nine positions versus the five positions run during previous tests.

Finally, the Mach 2.99 sample trajectory axial force data is not provided here because, in all cases, the axial force was within –3.0% to +10.0% of the isolated LGBB for both the orbiter and booster.

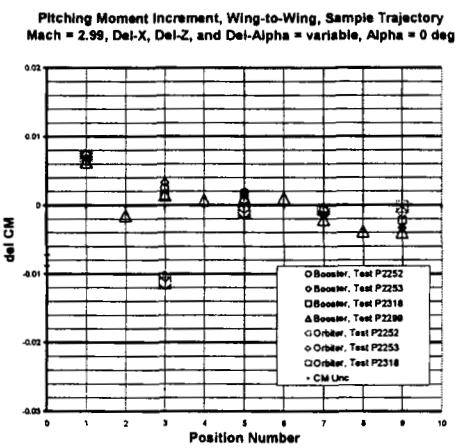

Figure 19. Pitching Moment Increment, Wing-to-Wing, Sample Trajectory

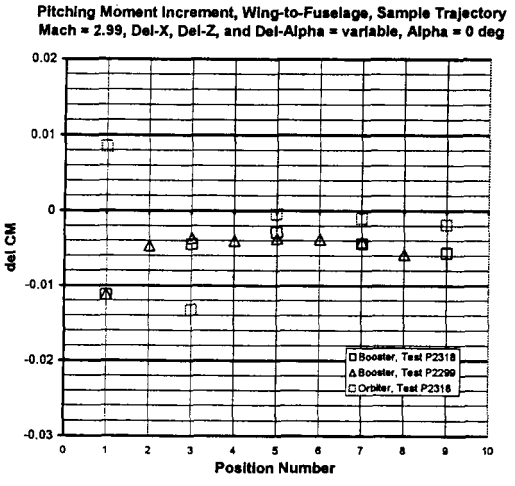

Figure 20. Pitching Moment Increment, Wing-to-Fuselage, Sample Trajectory

Unsteady Surface Pressure Results

As mentioned earlier, the orbiter model was instrumented with 20 miniature pressure transducers with the objective of measuring both the steady and unsteady static pressure on the surface of the fuselage and wing. Table 1 below provides the locations for the transducers. The fuselage pressures were located on the lower surface at the centerline; the wing transducers were at 50% span on the windward (lower) and leeward (upper) sides of the wing.

Table 1. Unsteady Pressure Transducer Locations

Measurement ID	Location	% Lref from Nose Leading Edge
PU-01	fuselage	58.89
PU-02	fuselage	65.96
PU-03	fuselage	73.04
PU-06	fuselage	96.00
PU-07	fuselage	101.33
PU-08	wing WW	81.65
PU-09	wing WW	86.04
PU-11	wing WW	94.81
PU-13	wing LW	81.65
PU-14	wing LW	83.85
PU-15	wing LW	86.04
PU-16	wing LW	88.24
PU-17	wing LW	90.43
PU-18	wing LW	92.62
PU-19	wing LW	94.81
PU-20	wing LE	n/a

Key:
WW -- windward side of wing
LW -- leewardside of wing
LE -- wing leading edge

Results for the unsteady (composite rms) surface static pressure are provided for the sample trajectory for the wing-to-wing configuration. Figures 21 and 22 show the unsteady composite RMS pressure for the wing-to-wing configuration for the windward and leeward transducers, respectively. The unsteady pressure is plotted as a delta-Cp'x100 computed by subtracting the composite rms for the isolate LGBB (p',iso) from the composite rms for the proximity case (p'), then dividing by the free-stream dynamic pressure (qinf) x 100. Note that transducers 4, 5, 10, and 12 are not shown because they were loss prior to or during testing or deemed outliers during post-test analysis.

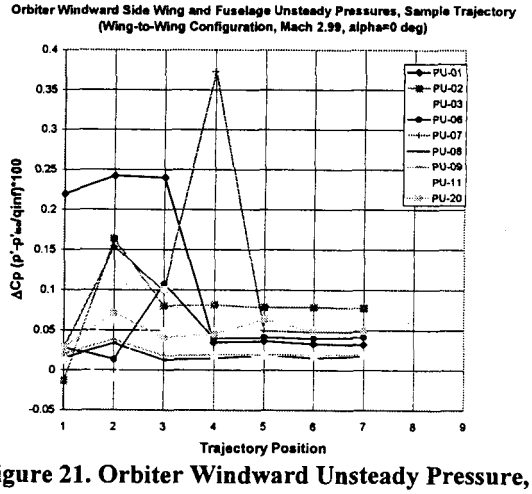

Figure 21. Orbiter Windward Unsteady Pressure, Wing-to-Wing, Sample Trajectory

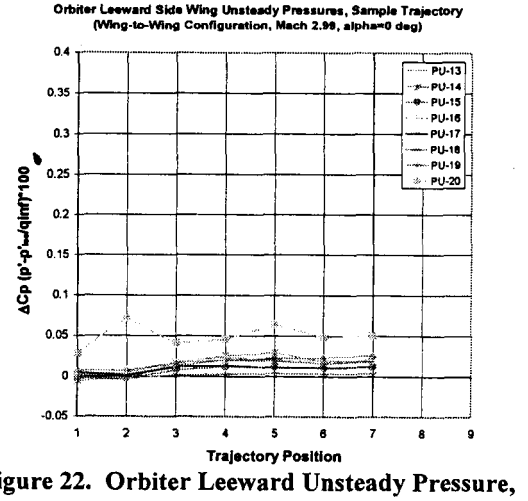

Figure 22. Orbiter Leeward Unsteady Pressure, Wing-to-Wing, Sample Trajectory

Discussion of Results

Z Trajectory

The schlieren and force and moment the Z trajectory are shown is figures 7, 9, 10, 11, and 12. In figure 7, the symmetric nature of the wing-to-wing Z trajectory is shown with the bow shocks and complex shock "train" between the orbiter and booster being symmetrical for all four positions. For the wing-to-wing configuration, the normal force slope with alpha for both the orbiter and booster is shown in figure 9 to be similar to the isolated over the full range of angle-of-attack. In figure 10, the orbiter and booster were shown to be statically stable in pitch at the first three positions changing to marginally stable at the furthest Z position.

In figures 11 and 12, the normal force and pitching moment increments at a stack alpha = 0 are shown. The increments for both the wing-to-wing and wing-to-fuselage configurations are shown. Again the symmetric nature of the wing-to-wing Z trajectory case is shown with the orbiter and booster normal force and pitching moment being equal at each position. In the wing-to-wing configuration, the orbiter had a normal force and pitching moment tending to separate the two bodies at all four positions (normal force and pitching moment were positive), and the booster had the same tendency except at the del-Z = 0.15 and 0.20 positions where pitching moment was negative. For the wing-to-fuselage configuration, only the booster data was acquired and is shown. The booster had a negative normal force and pitching moment (tending to push away from the orbiter) except at the del-Z = 0.2 position where pitching moment was positive. In all cases, the normal force and pitching moment were not back to their isolated LGBB values indicating that there was still measurable aerodynamic interference. This is clearly shown in the schlieren images.

Finally, the axial force was measured for both the orbiter and booster, and it showed an increase over the isolated LGBB by about 3% for the Z trajectory for an alpha equal to zero degrees.

Sample Trajectory

The schlieren, force and moment, and surface pressure results for the sample trajectory are shown in figures 8, 13 through 20, 21, and 22. Figure 8 shows the schlieren for positions 1, 3, 5, 7, and 9. Unlike the wing-to-wing Z trajectory case, the flow is only symmetrical at the 1 position with the orbiter and booster inverted in the tunnel and the booster "falling away". The schlieren also shows that the orbiter is outside the influence of the booster after position 5, whereas, the booster continues to be in the wake of the orbiter shocks. It should also be noted that by position 3 the booster's wing-side bow shock intersected the orbiter wing downstream of the orbiter moment reference point.

Since this trajectory is not symmetric for either configuration, both the orbiter and booster data is provided. In figures 13 and 14, the normal force for the orbiter and booster is shown to closely follow the isolated LGBB case for both the wing-to-wing and wing-to-fuselage configurations. For alpha = 0, the orbiter normal force was zero or positive for both configurations. For the alpha = 0 case, the booster normal force was zero or positive for the wing-to-wing configuration and zero or negative for the wing-to-fuselage configuration. This indicated that the normal forces on the orbiter and booster were tending to push the two bodies away from each other for this sample trajectory.

In figure 15, the complex nature of the pitching moment for the booster is shown for both the wing-to-wing and wing-to-fuselage configurations. For the wing-to-wing and wing-to-fuselage configurations, the booster is shown to progress from statically stable to unstable in the pitch direction. In figure 16, the orbiter is shown to be statically stable at all positions. With respect to the pitching moment for both configurations, only at position 1 did the orbiter and booster tend to want to separate at a stack angle-of-attack equal to zero.

In figures 17 and 18, the trend for the normal force to be equal to the isolated LGBB case at a stack angle-of-attack equal to zero is seen. As expected, the orbiter normal force tended toward the isolated LGBB value at position 5 and higher. Position 3 for the orbiter and position 9 for the booster showed the most difference from the isolated LGBB case being more positive for both the wing-to-wing and wing-to-fuselage configurations. This is interesting since one might think that position 1 would have the greatest normal force difference from the isolated LGBB.

Again, the complex nature of the pitching moments and the good test-to-test repeatability are depicted in figures 19 and 20 for a stack angle-of-attack equal to zero. As expected the orbiter pitching moment approached the isolated LGBB case for positions 5 and above. There was a large positive to negative change in the orbiter pitching moment from positions 1 to 2 for both the wing-to-wing and wing-to-fuselage configurations. From the schlieren video, this was shown to be caused by the booster wing-side bow shock intersection point on the orbiter wing traversing across the orbiter moment center, forward to aft.

The booster pitching moment at position 1 for the wing-to-wing configuration was positive and

coincided with the orbiter pitching as expected. For the wing-to-wing configuration, the booster pitching moment at positions 2 through 9 approached the isolated LGBB case with values less than and greater than the isolated case. For the wing-to-fuselage configuration, the booster pitching moment was lower than the isolated LGBB case for all positions with positions 1 and 2 having a negative value and tending to drive the booster away from the orbiter.

For both configurations, the booster pitching moment did not become equal to the isolated LGBB as the simulated sample trajectory approached position 9 indicating that the booster still had aerodynamic interference from the orbiter.

The repeatability from test-to-test is also shown to be good with some cases having three tests shown. During test P2299 the position resolution was increased from five to nine points. The data is shown to fill-in quite well with earlier test data.

Finally, the orbiter unsteady surface pressure data is shown in figures 21 and 22 for the wing-to-wing sample trajectory. As shown, the orbiter composite rms unsteady windward (side facing the booster) surface pressure with the booster in proximity was higher than the isolated case at five of the surface locations. Four of the five locations were on the fuselage with the most aft fuselage point having the maximum increase in unsteady pressure at position 4. Conversely, the wing leading edge and leeward surface unsteady pressures showed little to no increase over the isolated LGBB case.

Observations

Based on this work, the following observations were made:

1) The shock interactions between the orbiter and booster are complex with only the wing-to-wing configuration, Z trajectory providing a symmetric simplifying case to examine.
2) The measurement repeatability and test procedures used provided test-to-test data repeatability that was within the estimated uncertainties and sufficient for preliminary design. Accurate data at additional separation locations could be obtained with additional tests as required.
3) For the sample trajectory, the orbiter longitudinal forces and moment approached the isolated LGBB case, as expected, when the orbiter reached a position outside the booster shock influence.
4) For all cases examined, the change in normal force with alpha (normal force curve slope) was within 25% of the isolated LGBB normal force curve slope for alpha's from -14 to +18 degrees.
5) At a stack angle-of-attack of zero degrees, the normal force tended to separate the orbiter and booster. This was not the case for the pitching moment where the bow shock interaction determined the pitching moment direction.
6) For both the Z trajectory and the sample trajectory, the orbiter was statically stable to marginally stable at all positions in the pitch-plane. Conversely, the booster pitching moment was highly non-linear as a function of alpha and indicated that the booster was statically unstable at several separation positions.
7) For all cases examined, the axial force was within -3% to +10% of the isolated LGBB case.

Summary

In support of NASA's Space Launch Initiative Program, stage separation wind tunnel tests of a generic two-stage-to-orbit (TSTO) launch vehicle were successfully conducted in the MSFC Aerodynamic Research Facility. Test hardware, methods, and instrumentation were developed, including the application of miniature pressure transducers, and were shown to provide accurate results applicable to winged TSTO launch vehicles. For the bimese LGBB configuration, both wing-to-wing and wing-to-fuselage configurations were tested over a Mach number range from 2.74 to 4.96 and separation distances up to 80 percent and 35 percent of the body length in the vehicle X and Z coordinates, respectively. The Mach 2.99 longitudinal proximity aerodynamics for two trajectories were presented and discussed.

Acknowledgements

The authors would like to thank the MSFC ARF test team for the many hours of great testing provided. Thanks to Dynetics, Inc. for the design and fabrication of the models, and Kulite Semiconductor Products, Inc. for providing and installing the unsteady pressure transducers.

References

[1] Simon, Erwin H., "The George C. Marshall Space Flight Center's 14 x 14 Inch Trisonic Wing Tunnel Technical Handbook," NASA TMX-64624, November 5, 1971.